Analog Integrated Circuits and Signal Processing, 14, 275–296 (1997)

A Smart Sensor System for Carbon Monoxide Detection

G. C. CARDINALI[1], L. DORI[1], M. FIORINI[1], I. SAYAGO[1,2], G. FAGLIA[3], C. PEREGO[3], G. SBERVEGLIERI[3], V. LIBERALI[4], F. MALOBERTI[4], AND D. TONIETTO[4]

[1] *CNR-LAMEL, Via Gobetti 101, 40129 Bologna, Italy;* [2] *On leave of absence from: Laboratorio de Sensores, CSIC, Serrano 144, 28006 Madrid, Spain;* [3] *INFM, Department of Chemistry and Physics for Materials, University of Brescia, Via Valotti 9, 25133 Brescia, Italy;* [4] *Department of Electronics, University of Pavia, Via Ferrata 1, 27100 Pavia, Italy*

Received January 26, 1996; Accepted January 30, 1997

Abstract. This paper illustrates a smart sensor system for carbon monoxide detection. An innovative technological approach has been pursued to fabricate gas sensors on silicon substrate, compatible with IC fabrication. A mixed analog-digital electronic interface processes the outputs of three sensors to compensate relative humidity and interfering gases. Sigma-delta signal processing and low-frequency noise reduction techniques are used to minimize silicon area and to meet the required performance in a standard CMOS technology.

Key Words: sensors, sensor interfaces, sigma-delta converters

1. Introduction

It is well known that whenever combustion takes place with lack of oxygen, carbon monoxide (CO) gas is produced. This gas is extremely dangerous even at a low concentration and it must therefore be carefully monitored.

The working principles of solid-state devices used for CO detection are based on the conductance variation of the sensing layer or on the temperature increase in a heated element. Both effects are the results of chemical reactions between the substances to be detected and the material from which the sensor is made. However, CO sensors are intrinsically sensitive to interfering gases like alcohol, relative humidity, methane and many others [1]. The influence of interfering gases on the output of CO sensors can be as great as the contribution of the CO itself or even greater. This limits the use of conventional detection systems in most situations. To avoid this problem a multisensor system can be used. By combining signals generated by different sensors, we can obtain a signal which is proportional only to the CO concentration.

In this paper, we describe an innovative system for CO detection, featuring:

i) an array of three sensors, to detect CO, ethyl alcohol (C_2H_5OH) and relative humidity (RH);
ii) CO and alcohol sensing layers deposited on very thin dielectric membranes obtained by micromachining the silicon substrate (in view of a future full integration of the system), to reduce power consumption to a hundred milliwatts;
iii) analog electronic interface for signal processing and for temperature pulsed measurement to maximize sensor sensitivities.

The whole sensor system is outlined in Section 2. Section 3 describes the microstructure of integrated gas sensors, and Section 4 illustrates the electronic interface for control and measurement. Finally, Section 5 presents the results from the experimental characterization of single blocks.

2. System Overview

The system described in this paper is designed to detect the indoor presence of carbon monoxide. The target is to design a smart sensor system with the following characteristics: high reliability, low cost, reduced size and power consumption, high sensitivity to CO gas, reduced cross-sensitivity (lower false alarm rate), and reduced long-term drift. The sensor system must provide an alarm signal when the CO concentration exceeds a pre-defined threshold value (around 150 ppm), as well as a warning signal at half the alarm threshold. An additional output, proportional to the CO concentration, can be directed to a microprocessor unit to monitor the variation of CO concentration over time. To display the CO concentration in percent units of the alarm threshold, the resolution required of the sensor system is 7 bits.

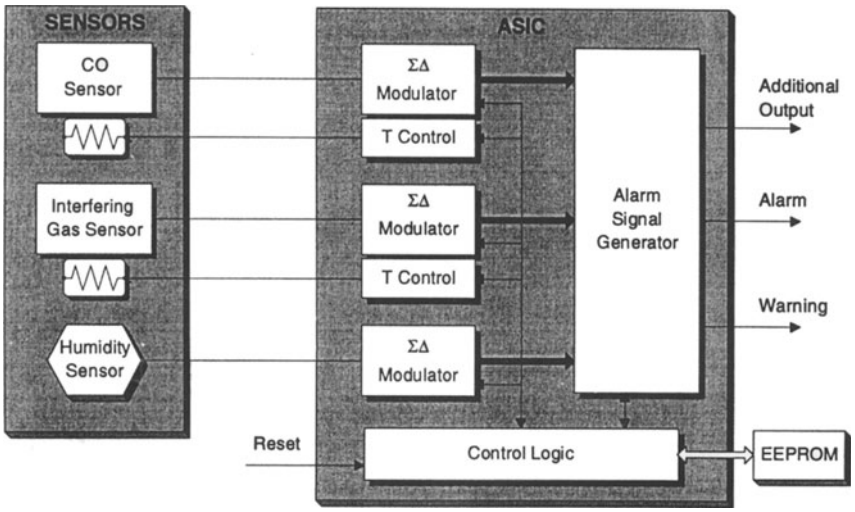

Fig. 1. Block diagram of the smart sensor system.

The smart sensor system is made up by a full-custom integrated circuit implementing the electronic interface and an array of three sensors. The array contains a commercial humidity sensor and two innovative microsensors for CO and interfering gas detection. Fig. 1 shows a block diagram.

The gas sensors are based on SnO_2 sensing layers that show a variation in resistance when gases are present. The SnO_2 film is deposited on a thin membrane realized on a silicon substrate using the bulk-micromachining technique. To increase CO selectivity, the two sensing layers are doped to enhance sensitivity to CO in the first device and reduce it in the second one.

As with other common interfering substances, air relative humidity (RH) also perturbs sensor conductance. This requires constant monitoring and compensation to guarantee the correct correlation between the sensor output signal and the CO concentrations. A low-cost capacitive sensor available on the market is used to this end [2]. However, the system architecture allows the discrete sensor to be easily replaced with an integrated humidity sensor.

The electronic interface is integrated in 1.2-μm CMOS technology. It carries out control and measurement functions, spanning from reference and clock generation to sensor temperature control and signal processing with oversampled techniques. The electronic interface has a high degree of programmability which can be exploited to adapt calibration and measurement parameters to different sensors based on the same detection principle (e. g. alcohol, methane).

3. Sensor Microstructure

Fig. 2 shows the microstructure of one of the two gas sensors. The sensing film is placed on top of a layer stack constituted (in order from bottom) by the membrane, the heater element, the passivation layer and the metal contacts.

Each of the above components is described in the following.

3.1. Sensing Layers and Related Technology

Solid-state CO detectors chemically react with the gases to be detected. The reaction produces a change in the conductance of the sensing layer or a temperature increase in a heated element (catalytic sensor). Catalytic sensors are low cost devices, but they have low selectivity and need high gas concentrations to work effectively.

The most widely used sensors in indoor applications are based on the first of these two solutions and depend on the properties of wide-gap semiconductive materials, such as SnO_2, deposited on suitable substrates. When a SnO_2 film is heated at $300 \div 400°C$ in air, it

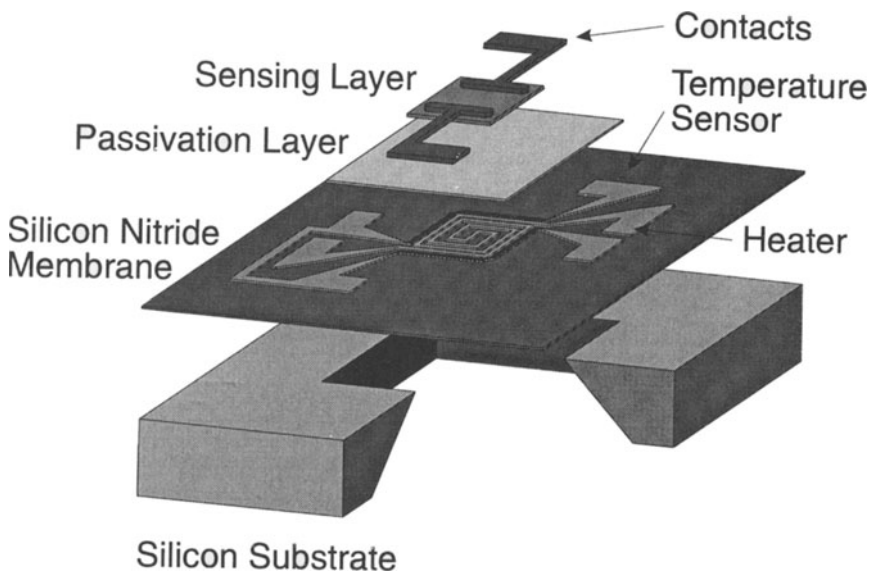

Fig. 2. Sensor device microstructure.

traps oxygen molecules on the sensor surface in the form of ions (O^-, O_2^-), lowering its overall electrical conductivity. If CO molecules are present in the surroundings, they react at the surface of the sensor leading to a charge injection that produces a conductivity variation, in agreement with the following reactions:

$$SnO_2 + e^- + \tfrac{1}{2}O_2 \rightarrow SnO_2(O^-)ad$$
$$SnO_2(O^-)ad + CO \rightarrow (SnO_2 + e^-)\, CO_2$$

The well-established Reotaxial Growth and Thermal Oxidation (RGTO) technique is ideal for the fabrication of this type of sensing layers [3–6]. RGTO sensors exhibit good sensitivity and time stability in their response, but they always exhibit some sensitivity to interfering gases, which could be present in ambient in high concentrations. It therefore becomes vital to discriminate between the response due to CO and to other interfering substances. To overcome this problem, a solution based on two sensitive layers has been considered. The first layer has been designed to be highly selective of carbon monoxide while the second is sensitive to ethyl alcohol, which is the most commonly found interfering gas.

To optimize the response of the sensor specifically designed to detect the CO, several solutions have been considered and incorporated into the thin film fabrication technology [7, 8]. A first approach entails the deposition of very thin catalyst layers (gold or platinum) on the surface of the sensing material. In addition, the use of an activated carbon filter has been considered. Indeed, experimental measurements have shown that a carbon filter drastically reduces the response to ethyl alcohol with concentrations in the range between 250 and 2000 ppm, while the magnitude of the sensor response to CO remains almost unaffected even at low concentration levels.

To reduce the effect of RH on the sensor response and to increase CO sensitivity, the sensor operating procedure has been optimized. The device is operated in a pulsed temperature mode (rather than at constant temperature) and thus the temperature is cycled between $120 \div 150$°C and $375 \div 450$°C every 60 s and 90 s, respectively. The conductance value is measured when the sensor temperature is in the lower range of the heating cycle. Experimental data collected with the sensor operating in this manner have shown that the effect of humidity is reduced and selectivity to CO increased in comparison with the standard operating mode. In addition, power consumption (depending on the pulsed duty-cycle) is lower.

Finally, to minimize the response drift due to aging ($1 \div 2$ years), the sensors were stabilized by thermal treatment at 500°C in the open air for two weeks.

Figs. 3–6 present experimental data showing the response of SnO_2 sensors under different conditions,

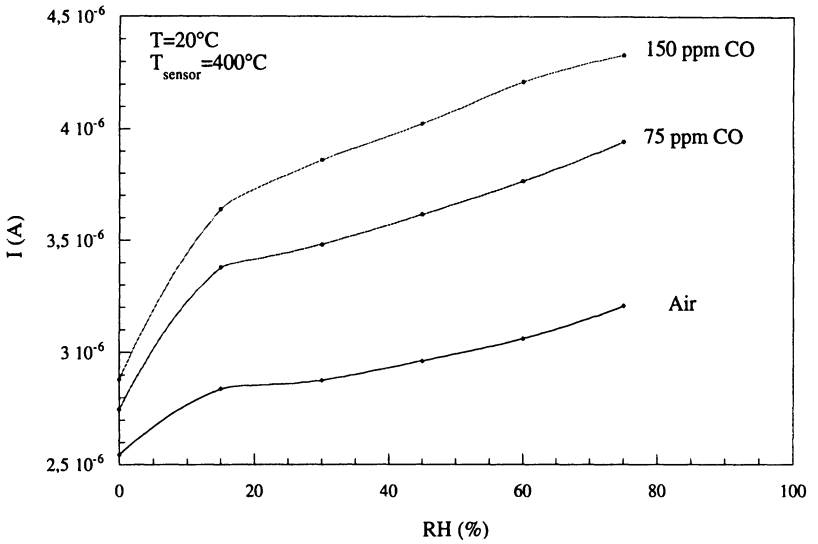

Fig. 3. SnO_2 Pt-RGTO film current (at 1 V bias) vs. RH at 0, 75 ppm, 150 ppm of CO in air. (The sensor case contained an activated carbon filter.)

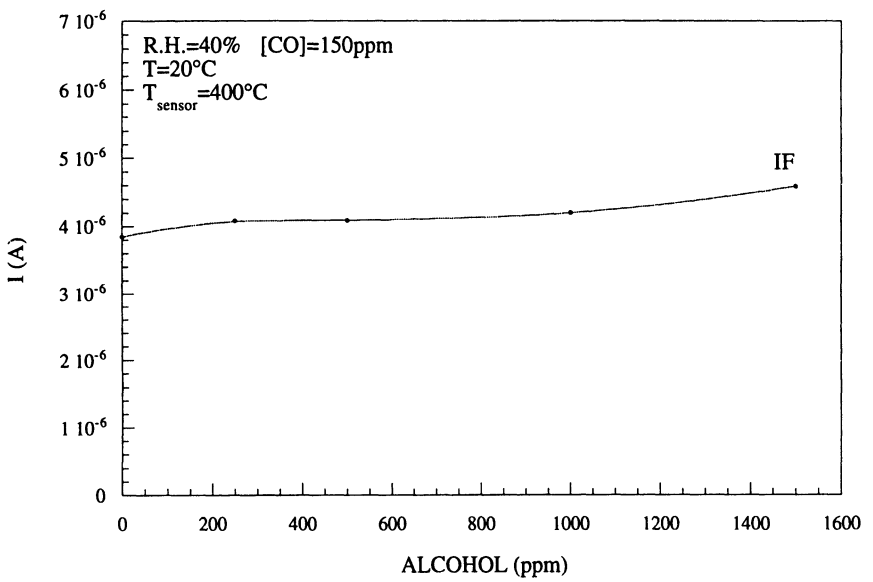

Fig. 4. Response of the sensor in Fig. 3 at fixed CO concentration (150 ppm) vs. C_2H_5OH concentration. (The sensor case contained an activated carbon filter.)

used to evaluate sensor behavior. The reported data and trends were employed in designing the electronic interface (see Section 4). For these measurements, the sensors were biased at 1 V, to obtain sensor conductance figures which are identical to the output current.

Fig. 3 shows how the relative humidity affects the output current of a SnO_2 Pt-doped RGTO sensor with an activated carbon filter on top. Measurements were carried out with CO concentrations set to 0, 75 ppm and 150 ppm, respectively. We can see that the output current increases as the RH increases, and that the slope of the current as a function of the RH does not depend on CO concentration (at least for the concentration range considered).

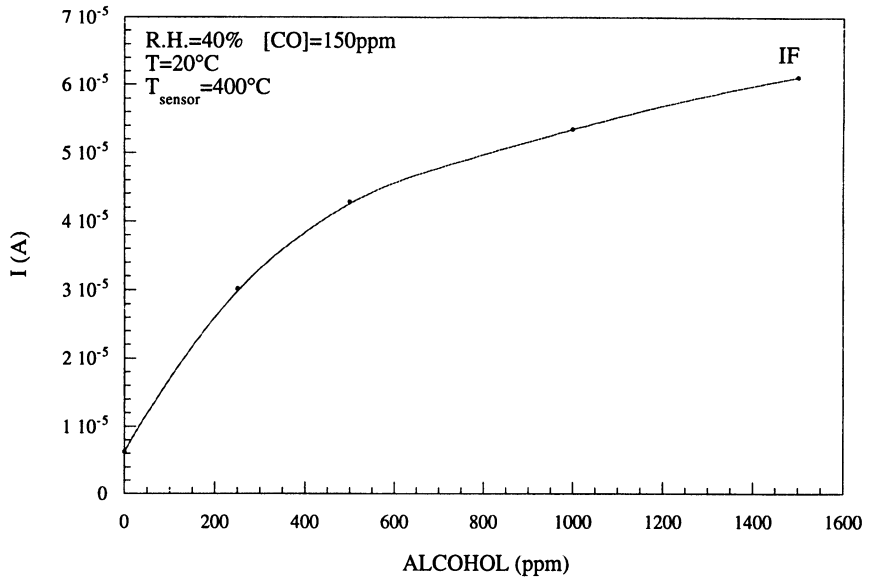

Fig. 5. SnO_2 Au-RGTO film conductance vs. C_2H_5OH concentration at 150 ppm of CO in air. (The sensor case did not have any activated carbon filter.)

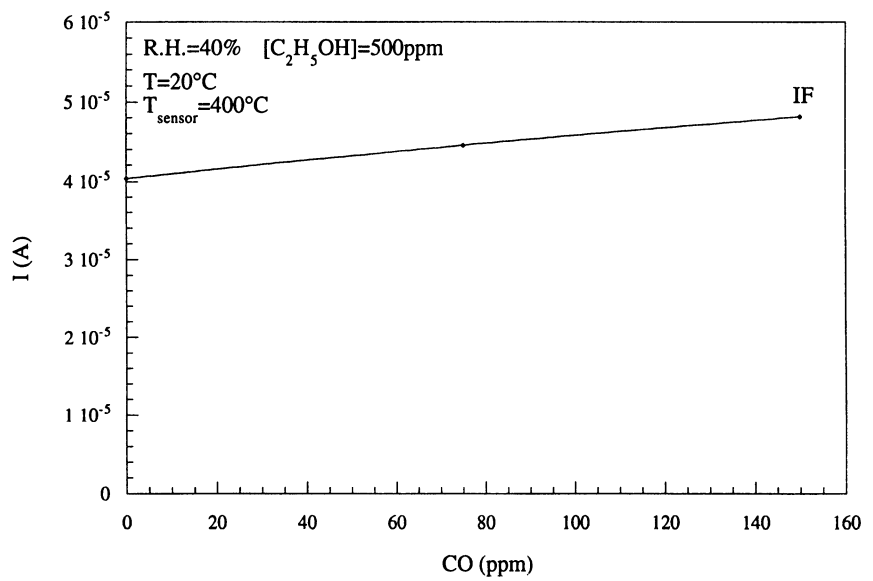

Fig. 6. SnO_2 Au-RGTO film conductance vs. CO concentration at RH = 40 % and $[C_2H_5OH]$ = 500 ppm in air. (The sensor case did not have any activated carbon filter.)

Fig. 4 shows the conductance variation of the same sensor, as a function of the ethyl alcohol content in the air. The CO concentration is set to 150 ppm. This figure shows that the SnO_2 Pt-RGTO sensor with a carbon filter is almost insensitive to the alcohol at concentrations below $500 \div 600$ ppm and slightly dependent on alcohol concentrations above that value.

Without the carbon filter, the sensor's response to a gas mixture similar to the one in Fig. 4 changes completely and exhibits a pronounced sensitivity to C_2H_5OH. Fig. 5 shows the output current of a SnO_2 Au-doped RGTO sensor, which exhibits a quite linear dependence for ethyl alcohol concentrations above 500 ppm.

Fig. 6 shows the SnO_2 Au-doped RGTO sensor response as a function of the CO concentration, at fixed amounts of RH (40 %) and C_2H_5OH (500 ppm). We can see that for CO concentrations from 0 to 150 ppm, the output current value of this sensor does not depend on the presence of CO in the environment.

The reported set of experimental data contains sufficient technical information to engineer and optimize the two sensors and ensure selective detection of both CO and ethyl alcohol.

3.2. *Thin Film Membrane on Silicon*

A thin film applied as mechanical support is an important feature in microsensor technologies. Essential membrane requirements can be summarized as follows:

i) mechanical stability;
ii) low stress material;
iii) low thermal conductivity;
iv) high chemical inertness under the KOH etchant (the same film must work either as etch-stop allowing the membrane to form or act as masking layer during the silicon bulk micromachining process);
v) film deposition process and material compatible with IC technology.

Many solutions have been proposed to realize thin film membranes [9–13]. They span from a single layer to a sandwich of dielectric layers like SiO_2/Si_3N_4/PSG, SiC. To fulfil these requirements without increasing fabrication process complexity, we modified the silicon nitride low pressure chemical vapor deposition (LPCVD) process to obtain a low stress membrane film. Membrane fabrication relies on a single lithographic step. Through reactive ion etching, the pattern of a positive photoresist layer reproduces mask apertures corresponding to the membrane in the silicon nitride deposited on the back side of a double polished silicon wafer (500 or 300 μm thick). After this lithographic step, the wafer is put in a KOH solution at $T = 80°C$ and bulk silicon is anisotropically removed through the silicon nitride openings. The process stops when the silicon nitride deposited on the front of the wafer is reached.

To optimize the mechanical properties of the micromachined membranes, their dimensions and fabrication processes have been considered with care. A number of membranes, with sizes ranging from 1×1 to 2×2 mm^2, were realized varying the parameters of the silicon nitride deposition process: temperature and gas ratio (diclorosilane/ammonia). A test was performed to investigate the mechanical stability of the membrane by applying a differential pressure. The membrane deflects in a blister-like shape and deflection is a function of membrane size and intrinsic film stress. Test results show that an increase in membrane area or in the gas ratio leads to an increase in deflection. On the other hand, the deposition temperature does not affect the deflection magnitude. Experimental characterization of fabricated devices shows that a 1.5×1.5 mm^2 membrane, 250-nm thick, breaks at a maximum overpressure of 100 kPa, while it deflects about 35 μm when a pressure of 40 kPa above the atmospheric pressure is applied.

3.3. *Heater Resistor and Temperature Sensor*

To set and measure the operating temperature of the gas sensitive layers, a heating resistor and a temperature sensor must be integrated on micromachined membranes. Both components can be fabricated by selectively etching the same conductive film deposited on top of the surface of the nitride film (the membrane). Sputtered platinum is the most widely used and characterized material for this type of application. It exhibits high stability in temperature cycles and a quite high temperature coefficient that ensures intrinsic temperature uniformity of the heater and provides a simple way to obtain a temperature measurement by monitoring resistance variations. The temperature sensor could be the heater itself, but design characteristics of the temperature control electronics suggest separate realization of these components would be more suitable. Indeed, at the operating temperature $T = 400°C$, the

optimum resistance value for the heater is 100 Ω, while the value for the temperature sensor is around 1 kΩ.

3.4. *Passivation Layer*

Following the scheme reported in Fig. 2, a passivation layer is needed to electrically insulate the heater from the sensing film. The resistance of the passivation layer must be high enough to ensure that leakage currents are not affecting the measurement of the sensible film conductance at working temperature (150°C $< T <$ 430°C) and at the applied bias (few volts). Moreover, the dielectric must have long term stability, to avoid lifetime reduction of the device due to Sn or Pt diffusion across the layer stack.

In standard processes, silicon nitride (Si_3N_4) and low temperature silicon oxide (LTO) films can be deposited using the LPCVD technique. Other possible passivation layers are: stress-free spin-on-glass (SOG) and titanium nitride (TiN).

Insulation properties of passivation layers have been thoroughly investigated by measuring the resistance between the sensing layer and the Pt resistors in several dielectric configurations. Experimental results show that tin diffusion through the passivation layer during the tin oxidation process (30 hours at $T = 600$°C) significantly degrades the insulating properties of a single passivation layer, making its resistance comparable to that of the sensor. From data reported in Table 1, the best choice is 1 μm of LTO on two SOG layers. Titanium nitride also offers very high electrical resistance, but its use is not recommended because it adds a tensile stress to the entire film stack and its realization process is more complex.

Table 1. Resistance of passivation layers

Passivation layer	thickness [nm]	resistance range
Si_3N_4	100	few kΩ
Si_3N_4	210	few MΩ
LTO	300	few kΩ
Si_3N_4 + TiN	235	$\gg$ GΩ
SOG + LTO	1500	$\gg$ GΩ
SOG + LTO + TiN	1750	$\gg$ GΩ

3.5. *Microstructure Design and Optimization*

As shown in Fig. 2, a platinum heater is placed at the center of a membrane, beneath the gas sensitive layer. The region where the sensing layer conductance is measured by means of an interdigitized shaped contact, is commonly referred to as the active area. The ratio between the edge of the square membrane and the edge of the active area is a key figure of the device design. The greater the ratio, the smaller the losses due to conduction heat transfer. Simulation results, carried out by means of the three-dimensional finite-element analysis program SOLIDIS [14], and experimental observations show that a reasonable trade-off between membrane size and conduction losses is obtained when this ratio ranges from 2 to 3. At the same time, convection and radiation losses depend on the size of the active area itself: the smaller the active area, the smaller the heating power required. On the other hand, the size of the active area depends on the shapes needed to optimize the response of the sensing film. An active area with a 700 μm side results from fabrication constraints. Starting from this active area and considering a 1500 μm membrane side, the heating power needed to raise the temperature of the active area to $T = 400$°C is calculated at about 100 mW.

To define heater geometry, the temperature distribution inside the active area was considered. Good uniformity is required to optimize the sensing layer detection mechanism. The performance of variously shaped heaters was evaluated by numerical simulation and by means of experimental measurements. The meander-shaped heater, widely proposed in the literature, exhibits poor temperature uniformity. This is probably due to the fact that the heating power per unit area is almost uniform, while heat exchange follows a quasi-radial distribution. An average gradient of 0.4°C/μm was obtained. Better results have been achieved by the double spiral shaped resistor shown in Fig. 7(a). The spiral layout has a variable pitch, to account for the distribution of heat losses inside the device active area. Fig. 7(b) shows the simulated temperature distribution, obtained with SOLIDIS. A minimum gradient of about 0.2°C/μm has been obtained.

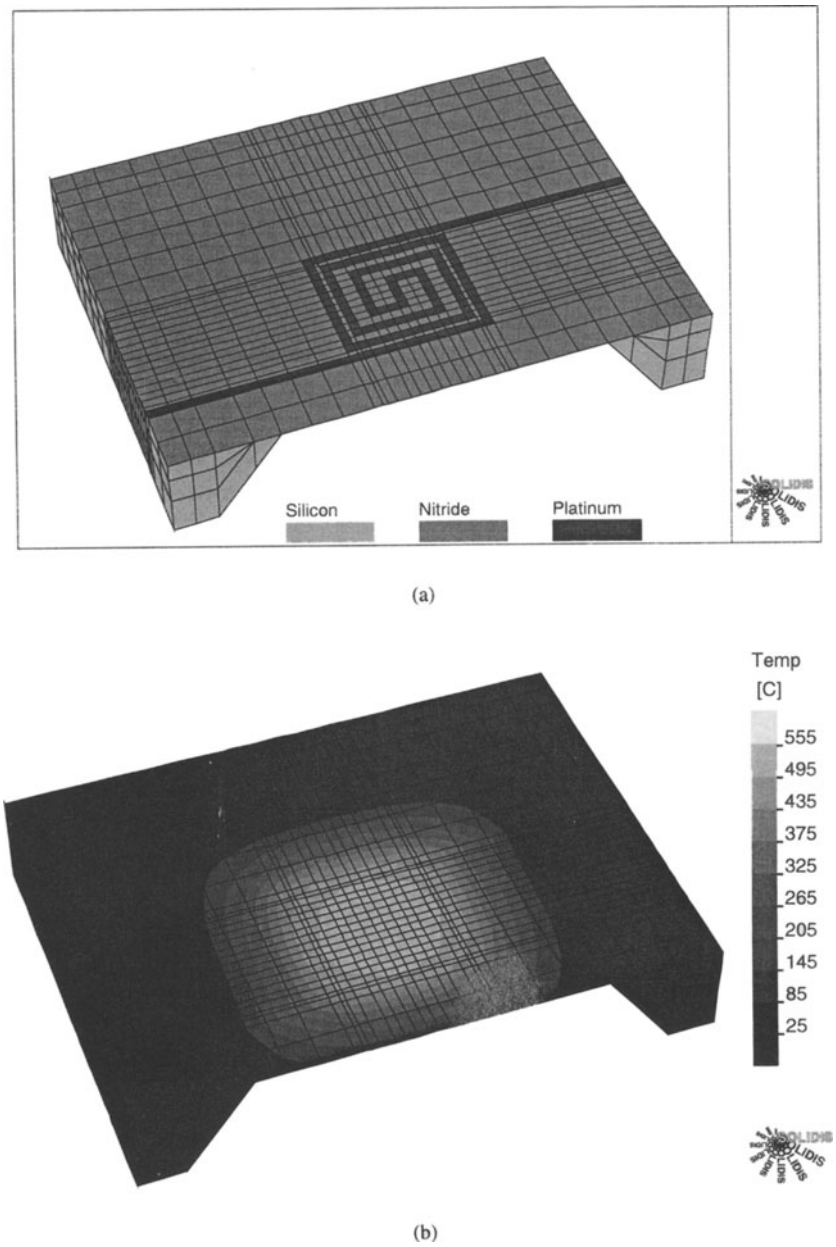

Fig. 7. Simulation results of a double spiral shaped heater: (a) geometry; (b) temperature distribution.

4. Design of the Electronic Interface

The main target in the design of control and measurement circuitry was achieving the best trade-off between performance and costs. To this end, the whole electronic interface was realized using a 1.2-μm CMOS technology and it was made as flexible as possible to easily conform to sensor characteristics and the requirements of the external alarm system.

The electronic driving circuitry will perform the following four main functions.

i) *Control logic.* Flexibility and programmability during control and measurement steps must be ensured.

ii) *Reference voltage generation.* Accurate voltage references must be generated for control and measurement.
iii) *Heating control.* During heating cycles, maximum accuracy and stability of the temperature is required.
iv) *Measurement and compensation circuitry.* This function is based on $\Sigma\Delta$ A/D conversion and on bitstream signal processing. This kind of elaboration requires a minimum amount of electronic circuitry to compensate spurious signals generated by interfering gases.

Fig. 8 shows the block diagram of the electronic interface IC.

4.1. Control Logic

Given the strong dependence of sensor behavior on the operating temperature, measurement and control require a high degree of flexibility to optimize system performance for different sensors. Therefore the control logic must allow the timing and duty cycles of heating steps to be changed, as well as the number and timing of measurements.

The timing section employs a 32 kHz quartz oscillator to generate a master clock signal with maximum stability. As shown in Fig. 8, the 32-kHz crystal is the only external component of the timing section. Two binary numbers corresponding to the length of each cycle are stored in the EEPROM (Fig. 1) to control the programmability of the heating cycles. Since the time interval of each cycle will not exceed 128 s, and a time resolution of 0.5 s is considered satisfactory, the master clock is divided by 2^{16}, and the output of a synchronous 8-bit counter is compared with the memory contents. A toggle flip-flop switches between two states and generates the control waveform with the requested duty-cycle. Measurement steps are timed and controlled in the same way.

4.2. Reference Voltage Generation

A voltage reference generator is needed both to measure the conductance of the sensors and in heating control. Such a voltage reference must have two important key features:

i) high temperature stability, because the pulsed mode operation of the heater may introduce temperature swings in the control circuitry.
ii) high rejection to supply variation, because a high voltage swing in the power supply may occur between low and high temperature cycles.

These two requirements are met by the band-gap voltage generator shown in Fig. 9. This circuit uses the base-emitter voltage V_{BE} of a vertical bipolar transistor (parasitic PNP BJT in N-well CMOS technology) to generate a reference voltage [15, 16]. It is well known that the V_{BE} voltage has a negative temperature coefficient. To compensate such a variation, the circuit relies on the positive temperature coefficient of ΔV_{be}. The ratio R_1/R_3 is selected to cancel the first order temperature effects. Low resistance values are used to minimize the silicon area required. The nominal reference voltage is 1.205 V. The layout of passive components has been carefully designed, to minimize mismatch effects. The variation of the generated voltage is less than 1 mV within a 70°C temperature range, and is less than 0.2 mV for a 1 V supply variation.

4.3. Heating Control

To operate in temperature pulsed mode, temperature stabilization is needed during heating cycles. As explained before, the heating system is constituted by two sputtered platinum resistors: the first is the heating resistor R_h, while the second is the measuring resistor R_m. Their nominal resistance values are 100 Ω and 1000 Ω, respectively. The operating temperatures are 400°C and 150°C. To reach 400°C during the heating cycle, at least 100 mW must be supplied to the heating resistor, that means that a current of 33 mA must be supplied by the control system. To furnish the heating current, a special output stage is added to a conventional single stage mirrored amplifier. The output stage consists of an open-drain PMOS transistor with $W/L = 1000$. The heater is connected to the drain to optimize the voltage swing.

Temperature is controlled through an "on/off" switching circuit. The basic idea is to have, for a given temperature, a reference resistor R_{ref} which has the same resistance as that expected for the measuring resistor.

Hence R_m is compared with the reference resistor and the power is switched on (off) if R_m is smaller (higher) than R_{ref}. The designed circuit implementing this control scheme is shown in Fig. 10. The tem-

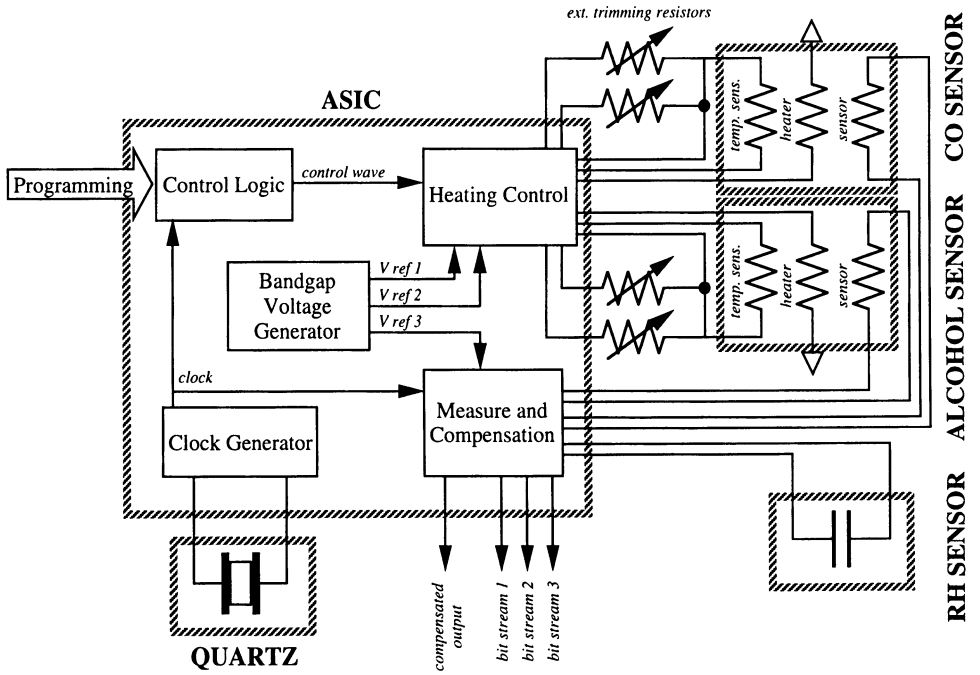

Fig. 8. Block diagram of the electronic interface circuit.

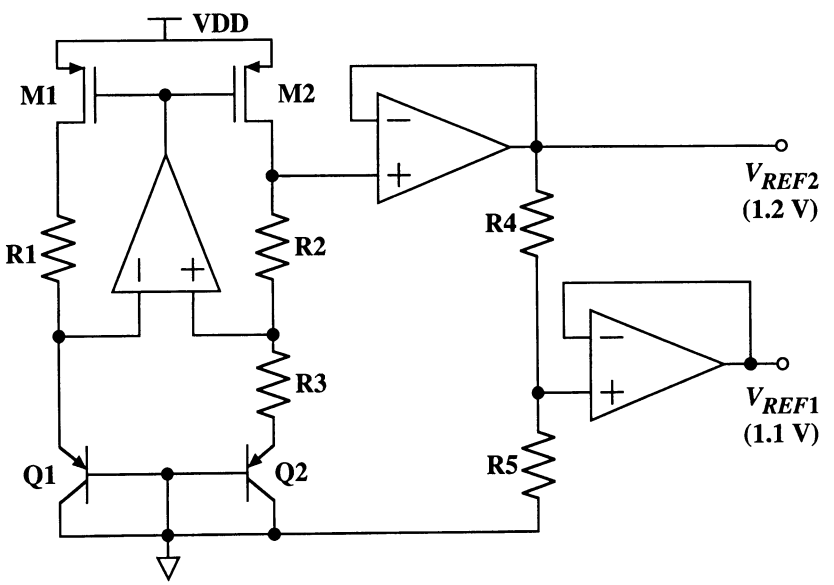

Fig. 9. Band-gap reference voltage generator.

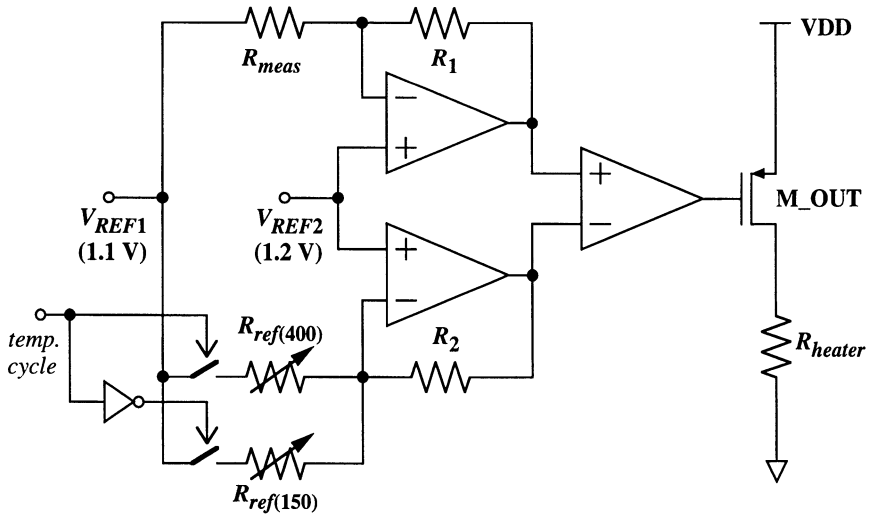

Fig. 10. Scheme of the "on/off" temperature control loop.

perature cycle is selected by switching between two reference resistors, according to the control logic signal. Let us suppose that the system has to perform the cycle at $T = 400°C$. Since the temperature is lower, the value of the sensing resistance R_m is smaller than its reference value, $R_{ref(400)}$. The output of the comparator assumes the high state, and power is switched onto the heater. When the temperature exceeds 400°C, the value of R_m becomes greater than the reference temperature and the comparator switches off the heating element. In this control scheme the output PMOS transistor behaves like a switch. A quite large output dynamic range is achieved, and the supplying power capability is considerably increased.

The temperature accuracy of the proposed control circuit depends on the matching between the reference and the measuring resistors. To account for deviations of real parameters from design values, the two reference resistors are discrete components (e. g. two multitwist trimmers) external to the ASIC. The system can be set to cycle between two given temperatures simply by adjusting the values of these resistors.

Computer simulations confirmed that the design specifications are also met in worst case conditions. A temperature control accuracy of about 2°C is achievable if a tight thermal link exists between the heater and the temperature sensor. This condition is satisfied in the device considered, due to the reduced dimensions of sensor microstructures.

4.4. Measurement and Compensation Circuitry

To obtain an electrical output which is only proportional to the CO concentration, the electronic interface must compensate effects produced by alcohol and by humidity on the SnO_2 sensor. Before considering how the conductance variation is converted into a readable signal, it is worthwhile to analyze how such compensation can be executed. The compensation scheme must take into account how interactions between interfering gases and the sensing layer influence the response of the sensor itself.

Let us denote the output of a CO sensor with an activated carbon filter on top with S_{CO}, the output of a sensor without a filter (specifically designed to reveal the presence of C_2H_5OH) with $S_{Alcohol}$, and the output of the humidity sensor with S_{RH}.

By considering only signals from the CO and C_2H_5OH sensors, we can write the following first-order equation set:

$$\begin{cases} S_{CO} = a_1 \cdot [\mathrm{CO}] + b_1 \cdot [\mathrm{C_2H_5OH}] \\ S_{Alcohol} = a_2 \cdot [\mathrm{CO}] + b_2 \cdot [\mathrm{C_2H_5OH}] \end{cases} \quad (1)$$

where square brackets [] are used to denote the gas concentrations.

The equation set (1) can easily be solved to express [CO] as a linear combination of signals S_{CO} and

$S_{Alcohol}$, as follows:

$$[\mathrm{CO}] = \frac{b_2\, S_{CO} - b_1\, S_{Alcohol}}{b_2 a_1 - b_1 a_2}.$$

It is well known that this kind of operation can be executed using $\Sigma\Delta$ techniques. Mathematical operations are performed on high-frequency bitstreams generated by second-order $\Sigma\Delta$ modulators from the sensor outputs [17, 18]. The resulting output bitstream is integrated to obtain low frequency samples of the CO concentration evaluated. A diagram of signal processing is illustrated in Fig. 11. The $\Sigma\Delta$ modulator architecture is described in [19].

Now let us consider how the results of prototype sensing layer characterization fit the first-order equation set (1).

By comparing Figs. 5 and 6 we can see that the conductance of the alcohol sensor is much more dependent on C_2H_5OH concentration than on CO concentration. This means that the conductance dependence on the CO concentration can be neglected, and we can assume that this sensor is sensitive only to ethyl alcohol. Curves of conductivity as a function of alcohol concentration (Fig. 5) exhibit a logarithmic behavior that becomes linear when the ethyl alcohol concentrations are larger that 500 ppm. Hence in the second equation the coefficient a_2 is set to zero.

Another point to be emphasized is the following. From Fig. 4, we can see that the conductivity of the sensor with carbon filter is practically insensitive to ethyl alcohol below 500 ppm, while above the 500 ppm value it shows a weak linear dependence. Hence, the coefficient b_1 in the first equation has to be set to zero when the C_2H_5OH concentration is below 500 ppm and set to the appropriate value for higher alcohol concentrations. This means that the effects of alcohol on the sensor conductance need only be compensated with concentrations exceeding 500 ppm. Moreover above this threshold value the conductance can be linearly compensated.

The conductance variation as a function of the relative humidity can be processed in a similar way. From Fig. 3 we can see that the CO sensor behaves linearly with RH values in the range $25 \div 90$ %. The same trend has been observed for the interfering gas sensor. This means that humidity effects can be easily compensated in both sensors by using the procedure described above. The capacitive sensor used to measure the RH is insensitive to CO as well as to C_2H_5OH.

To conclude, the following set of linear equations constitutes a good model of actual sensor behavior:

$$\begin{cases} S_{CO} = a_1 \cdot [\mathrm{CO}] + b_1 \cdot [\mathrm{C_2H_5OH}] + c_1 \cdot [\mathrm{RH}] \\ S_{Alcohol} = b_2 \cdot [\mathrm{C_2H_5OH}] + c_2 \cdot [\mathrm{RH}] \\ S_{RH} = c_3 \cdot [\mathrm{RH}] \end{cases} \quad (2)$$

By solving the equation set (2), we can express [CO] as a linear combination of the three signals S_{CO}, $S_{Alcohol}$, and S_{RH} as follows:

$$[\mathrm{CO}] = \frac{1}{a_1}\left(S_{CO} - \frac{b_1}{b_2} \cdot S_{Alcohol} - \left(\frac{b_2 c_1 - b_1 c_2}{b_2 c_3}\right) \cdot S_{RH}\right)$$

This operation can be performed directly on bitstream signals. However, it is worth noting that the multiplication in time domain corresponds to a convolution in z-domain. This means that the result of a multiplication of two noise-shaped bitstreams in time domain is a non noise-shaped waveform [18]. Consequently multiplications must be performed before bitstream generation. The simplest method is to multiply the analog signal by a bitstream corresponding to the multiplication coefficient [20, 21]. Conversely, two bitstreams can be added using very simple digital circuitry without losing the noise shaping benefits [17, 18, 22–24].

The block diagram of the measurement interface is illustrated in Fig. 12. Three 8-bit digital coefficients K_1, K_2 and K_3, defined on the basis of sensor characterization, are converted into bitstreams by three digital-to-bitstream $\Sigma\Delta$ converters. The impedance variations of the three sensors are sampled according to compensation coefficients and converted into three bitstreams by analog-to-bitstream second-order $\Sigma\Delta$ converters. The resulting bitstreams are added to obtain a single bitstream that can be low-pass filtered using a simple digital accumulator. Bitstreams are added using the interleaving technique [23]. Alternatively, three input stages could be used in a single $\Sigma\Delta$ modulator as proposed in [21], but this approach limits the flexibility of the whole system.

Resistive sensors are directly connected to the first stage of the $\Sigma\Delta$ converter, as illustrated in Fig. 13. A precise voltage reference is applied to the sensor, thus obtaining a current signal which is proportional to the sensor conductance. The sensor signal is chopped by the digital generated bitstream and integrated into the first stage of the $\Sigma\Delta$ modulator. In this manner the compensation coefficients are multiplied in mixed analog-digital domain, maintaining the noise-shaping characteristics of modulator outputs [18, 20].

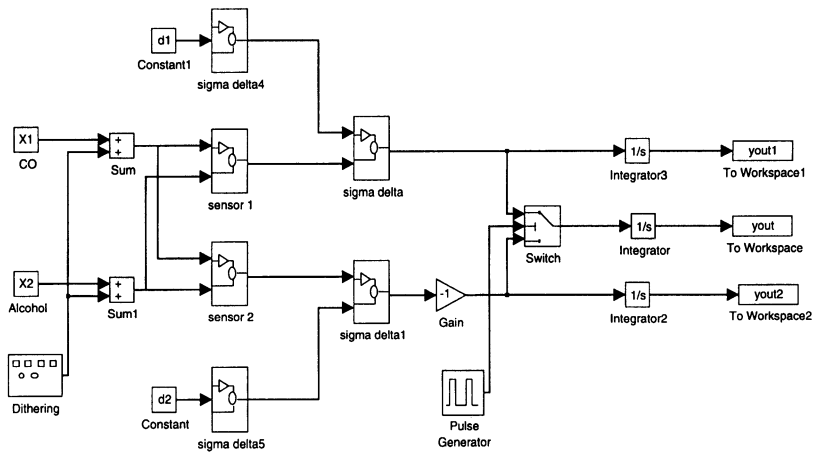

Fig. 11. Scheme of alcohol compensation.

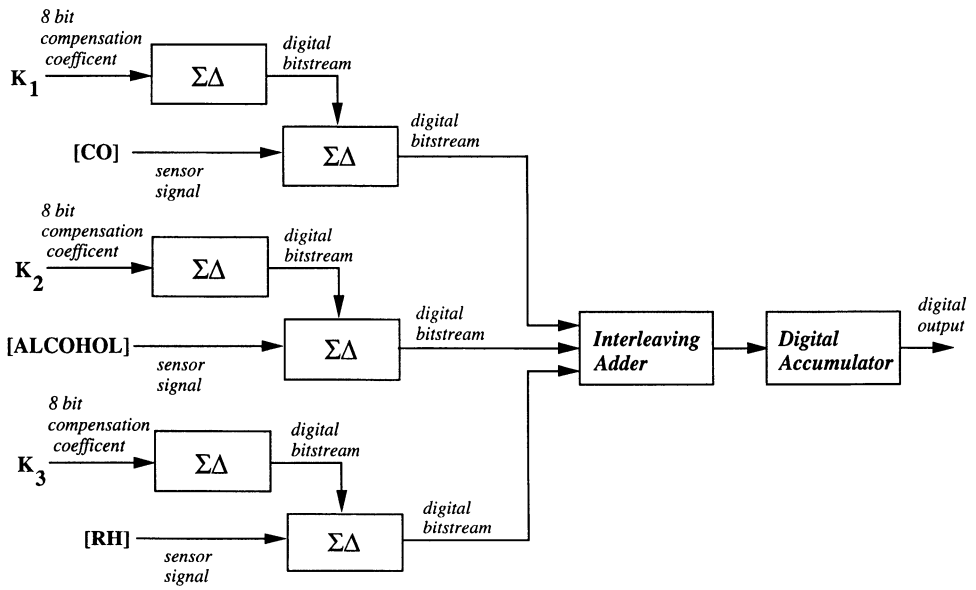

Fig. 12. Block diagram of the measurement interface circuit.

Conductance variations must be converted into readable signals by taking into account problems due to offset and flicker noise. Flicker noise and offset were cancelled using a sampled data auto-zero technique. During the auto-zero phase Φ_{AZ}, the inputs of the first integrator stage are connected to analog ground, the integrating capacitor is disconnected, and the integrator output is connected to the negative auxiliary input. The output voltage (equal to the input-referred offset and flicker noise) is sampled and held on the auto-zero capacitor C_{az}. During the successive clock phase the circuit acts as an integrator and the voltage stored on C_z, applied to the auxiliary input, cancels low-frequency flicker noise and offset components.

With the RH capacitive sensor we have a problem due to the large value of the sensor capacitance (around 100 pF). Such capacitance is not compatible with the integrating capacitor, since it would saturate the integrator output because of the over-large ratio C_{sens}/C_i. We overcame this problem using the circuit shown in

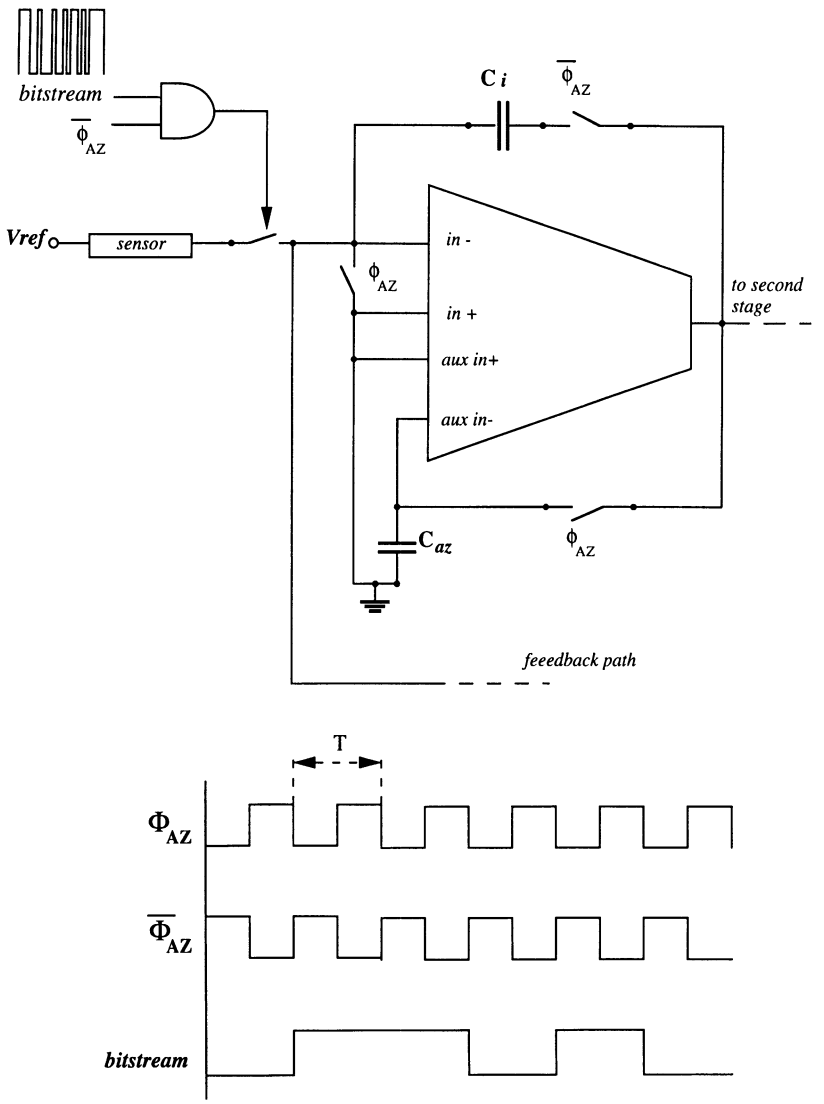

Fig. 13. Scheme of conductance measurement interface with auto-zero compensation.

Fig. 14. An additional capacitance (the reference capacitor C_{ref}) is switched like the RH sensor, but towards a voltage opposite to the sensor bias voltage. Consequently the charge injected into the integrating capacitor is:

$$Q = \Delta C \cdot V_{ref}$$

where

$$\Delta C = (C_{ref} - C_{sens})$$

This operation prevents integrator saturation.

High-level simulations of the measurement interface have been performed using MATLAB [25] and TOSCA [26].

Fig. 15 illustrates the results of the TOSCA simulation of the multiplication of a sinusoidal waveform by a constant coefficient. From the power spectral density of the resulting bitstream, we see the typical noise-shaping characteristics exhibiting a low-frequency noise level 60 dB below the signal. Fig. 16 illustrates the resulting spectrum of a chopped resistor measurement, obtained by circuit level simulation in time domain and fast Fourier transform (FFT). The two

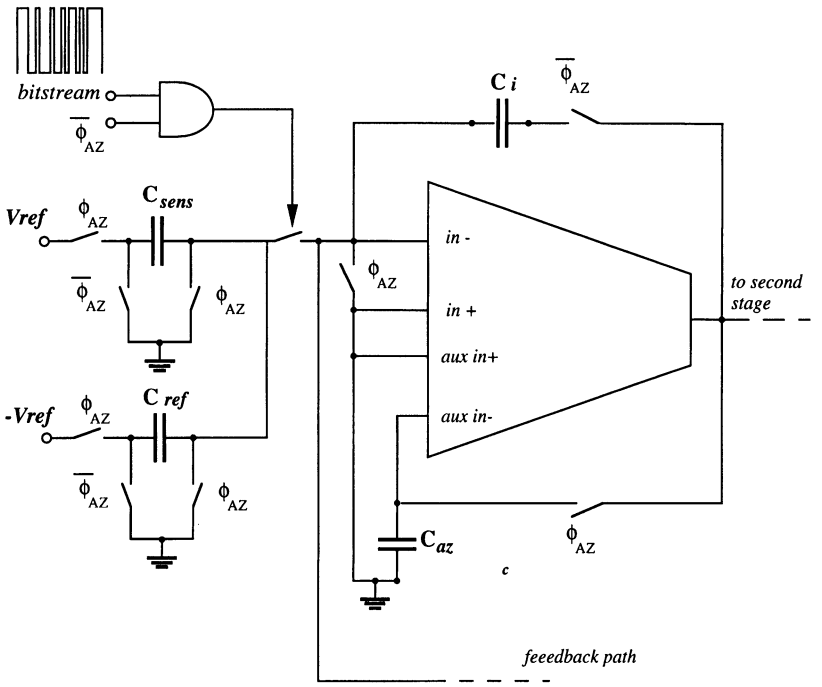

Fig. 14. Scheme of capacitance measurement interface with auto-zero compensation.

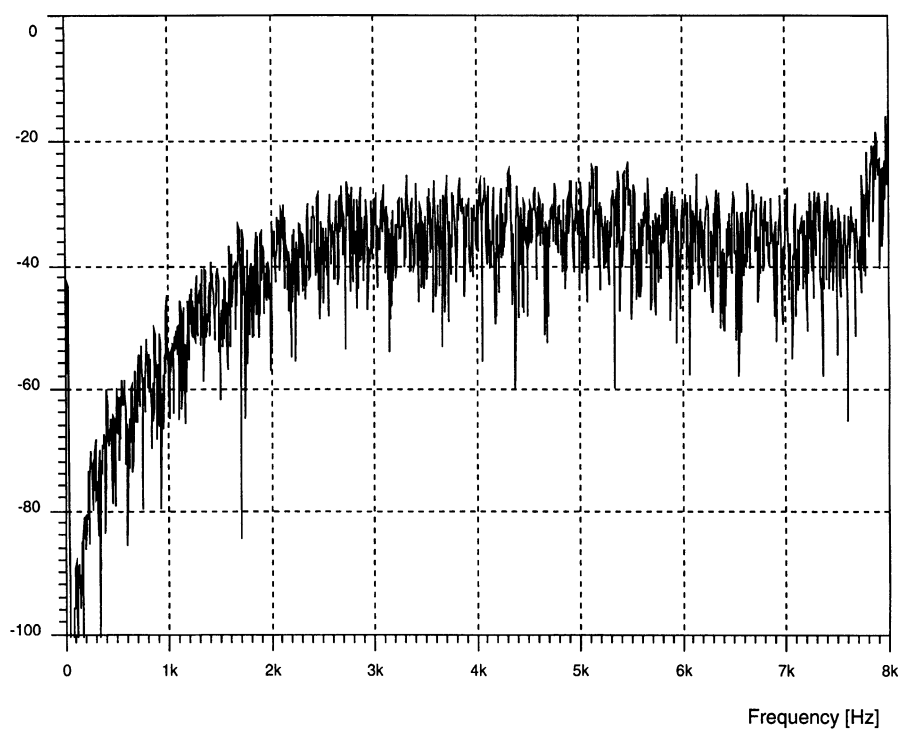

Fig. 15. Spectrum of the bitstream signal for a single sensor output (TOSCA simulation).

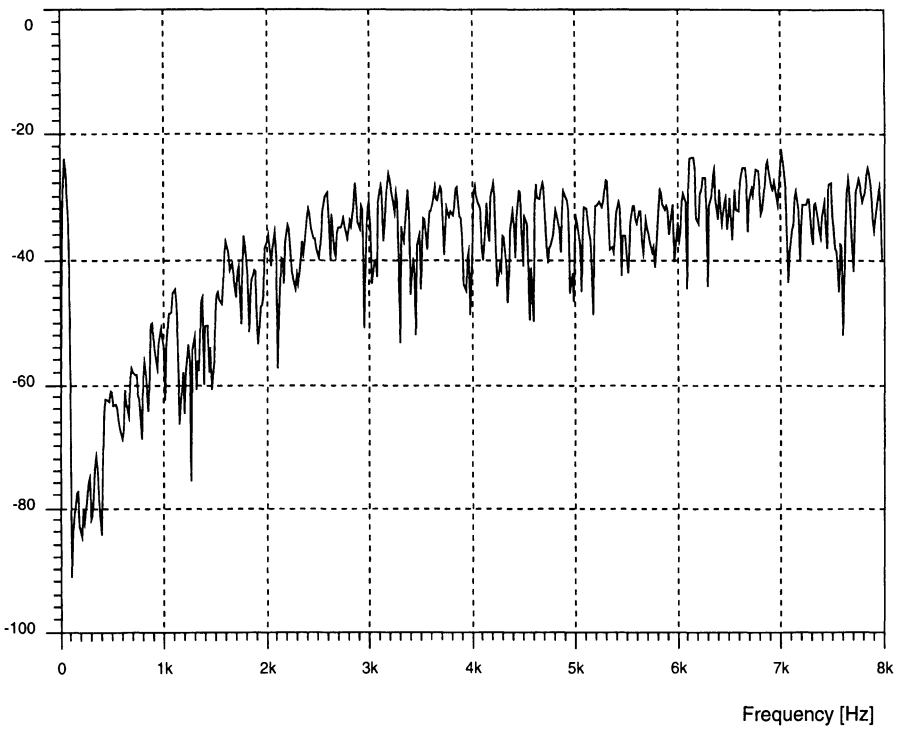

Fig. 16. Spectrum of the bitstream signal for a single sensor output (circuit-level simulation).

simulation results are in good agreement, and demonstrate the validity of the proposed approach for gas sensor signal processing.

5. Experimental Results

To evaluate sensor performance under different operating conditions and to optimize the whole system, the basic components have been fabricated and characterized separately. This section describes some experimental results allowing estimation of system behavior.

5.1. *Characterization of the Microstructure*

The blister test was also used to establish the maximum pressure that the Si_3N_4 membrane can sustain without breaking. This is useful in estimating the long-term membrane stability under operating conditions. The stress was applied by ramping a differential pressure up to one quarter of the breaking pressure, at a frequency of 100 cycle/min. The number of applied cycles was about 200000, equivalent to 1 year in pulsed temperature mode, with cycles of 150 s. To evaluate the magnitude of the stress applied, we point out that the membrane, when heated at $T = 450°C$, deflects $1 \div 2$ μm while during the differential pressure test it was deflected by tens of microns. All the tested devices exhibited excellent mechanical stability and none broke during the tests, proving the long-term reliability of the membrane.

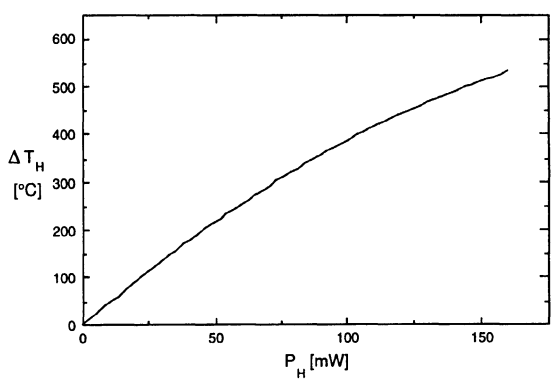

Fig. 17. Temperature increase in active area versus heating power.

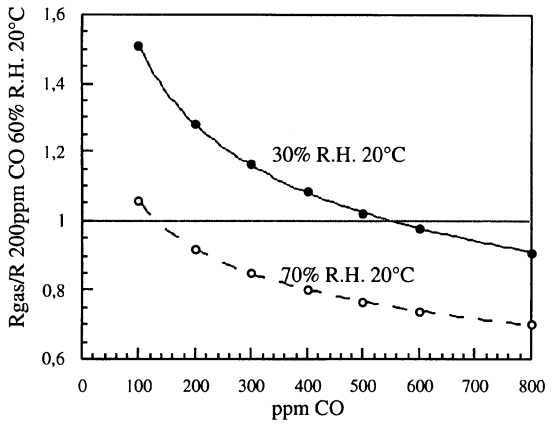

Fig. 18. Sensor response to CO concentration in constant temperature mode.

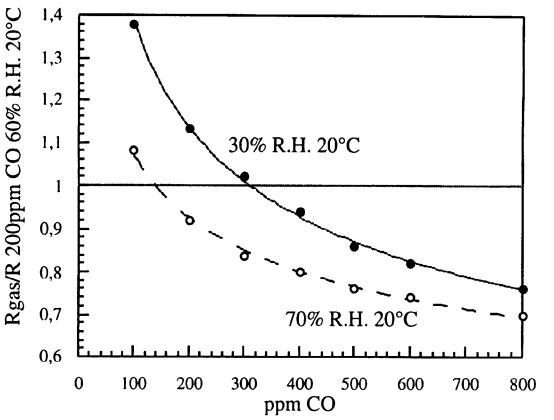

Fig. 19. Sensor response to CO concentration in pulsed temperature mode.

Further mechanical and electrical investigations were carried out on the complete structure (sensing layer included). In particular, an accelerated test was performed where the device was stressed pulsing the temperature between 200°C and 500°C each 2 s for 10 days. The results of the accelerated test have confirmed both the excellent mechanical stability of the whole system and the considerable endurance of the passivation layer.

The thermal behavior of the sensor microstructure has been thoroughly investigated by means of electrical and thermographic measurements. The dependence of the active area temperature on heating power has been determined (Fig. 17). A total power of about 100 mW is required to heat the active area at 450°C and 35 ms is the time interval needed to switch from 200°C to 500°C. The thermal variation of the platinum resistance has been investigated by electrical measurements performed on the real device and on test structures, maintained at a uniform and well-controlled tem-

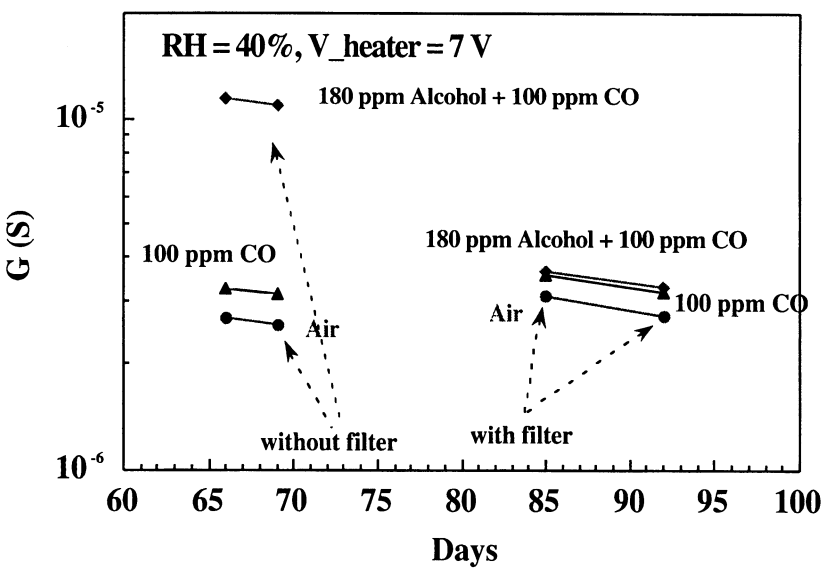

Fig. 20. Comparison of sensor responses to CO and alcohol (with filter and without filter).

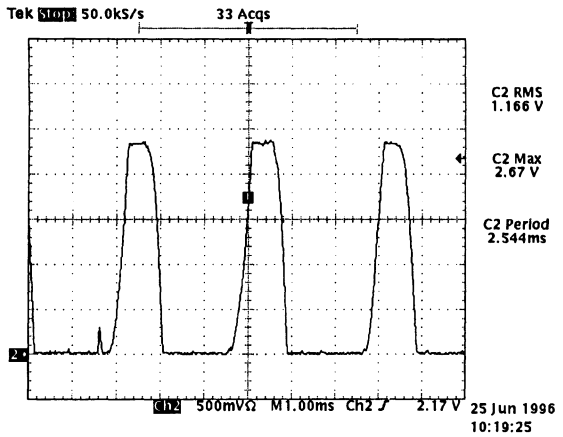

(a)

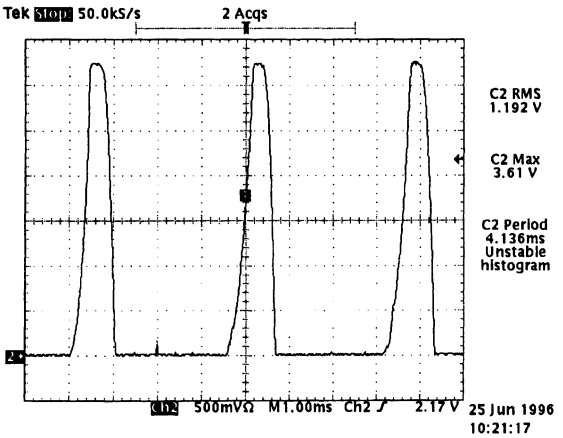

(b)

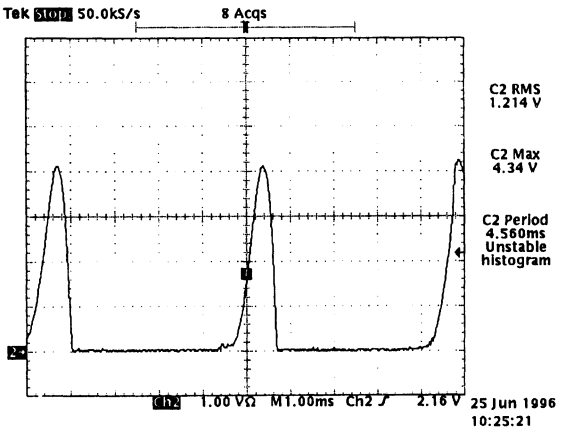

(c)

Fig. 21. Waveforms at the temperature control output for different values of supply voltage: (a) VDD = 3 V; (b) VDD = 4 V; (c) VDD = 5 V.

perature (±0.1°C). A positive temperature coefficient $\alpha = 2.71 \pm 0.06°C^{-1}$ has been evaluated.

5.2. *Characterization of the Sensing Films*

Experimental results on the stationary response of the sensing layers to different gas concentrations, are summarized on section 3.1. Here some aspects of the techniques used to reduce the sensitivity of the CO sensor to interfering gases, such as relative humidity and ethyl alcohol, are considered.

Figs. 18 and 19 show the responses of the same sensor at two different levels of RH using the constant and the pulsed temperature procedures. The sensor output is normalized to a reference condition of 200 ppm of CO and 60% of relative humidity. The pulsed temperature mode decreases the RH effect on the sensor response, without affecting CO sensitivity.

Ethyl alcohol interference can be minimized by using an activated charcoal filter (by SUPELCO, Inc.), positioned inside the sensor housing, in front of the sensing layer. Experimental results (Fig. 20) show that filtering is very effective, especially at low alcohol concentrations, without any appreciable efficiency reduction after several months of activity.

5.3. *Characterization of the Electronic Interface*

The blocks described in Section 4 have been characterized separately.

The on-off regulator which controls the membrane temperature has been proven to work properly, with a maximum output current equal to 40 mA. The maximum supplied heating power is 160 mW. The waveforms at the regulator output, with three different bias voltages: VDD = 3 V, 4 V and 5 V, are shown in Figs. 21(a), (b) and (c) respectively. From the figures, it is clear that the average heating power is independent of the bias voltage.

The three $\Sigma\Delta$ modulators have been tested separately. They have been proven to work properly and in agreement with the project specifications. Each $\Sigma\Delta$ modulator output is a bit stream, whose low-frequency analog content is proportional to the sensor conductance multiplied by the sampling coefficient.

Fig. 22 shows a single bit stream together with its power spectrum, obtained at the oscilloscope through Hanning window and 1024-point FFT. Noise shaping

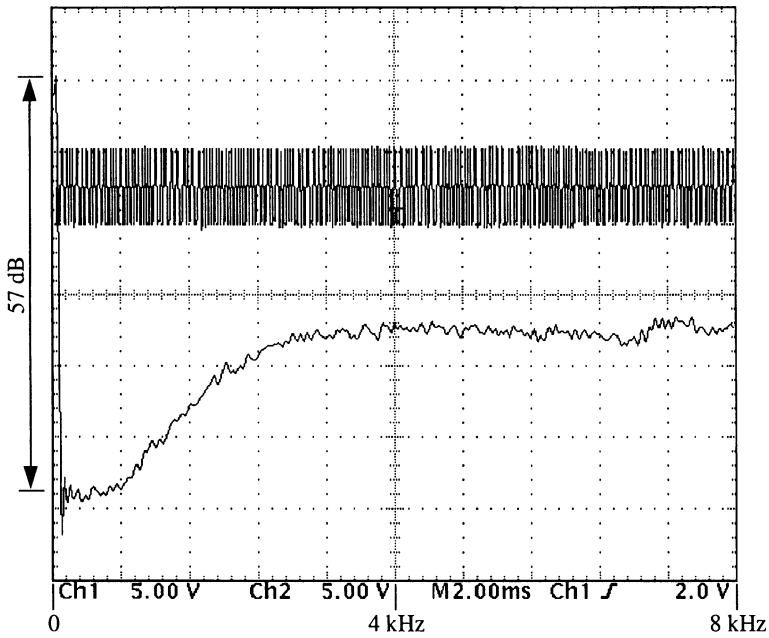

Fig. 22. A single output bitstream and its power spectrum (obtained at the oscilloscope through FFT).

is in good agreement with simulation results in Figs. 15 and 16. The low-frequency noise level flattens at −57 dB, due to the analog noise superimposed to the digital bit stream. The resolution required (7 bits) can easily be achieved by digitally filtering the bit stream with a narrowband low-pass filter. By using a simple comb filter that integrates the output bitstream over 0.5 s, the resulting signal-to-noise ratio is better than 40 dB, corresponding to a maximum error which is less than 1% of full scale.

6. Conclusion

This paper presented a multisensor architecture for carbon monoxide detection. Experimental characterization activities allowed us to define and, in some cases, to optimize the different technological steps involved in the realization of a sensor prototype. An electronic interface has been designed, both to generate the control signals and to process sensor outputs. By using signal processing in the bitstream domain, hardware complexity is greatly reduced whitout sacrificing system flexibility, while a satisfactory signal-to-noise ratio is maintained at low frequencies.

Acknowledgement

This work has been supported by the European Union under ESPRIT Projects 7500-MEPI (Demonstrator D-114) and 8795-AMFIS.

References

1. G. Williams and G. V. Coles, "NO_x response of tin dioxide based sensor," *Sensors and Actuators B* 15–16, pp. 349–353, 1993.
2. Philips, Technical Note 134 for Capacitive Humidity Sensor (catalogue number 2322 691 90001).
3. G. Sberveglieri, G. Faglia, S. Groppelli, and P. Nelli, "A new technique for preparing SnO_2 sputtered thin film gas sensors," in *Proc. Transducers '91, 6th Int. Conf. on Sensors and Actuators*, San Francisco, CA, USA, 1991, pp. 165–168.
4. G. Sberveglieri, "Classical and novel techniques for the preparation of SnO_2 thin film gas sensor," *Sensors and Actuators B* 6, pp. 239–247, 1992.
5. C. Di Natale, A. D'Amico, F. Davide, G. Faglia, P. Nelli, and G. Sberveglieri, "Performance evaluation of an SnO_2-based sensor array for the quantitative measurement of mixtures of H_2S and NO_2," *Sensors and Actuators B* 20, pp. 217–224, 1994.
6. G. Sberveglieri, "Recent developments in semiconducting thin-film gas sensor," *Sensors and Actuators B* 23, pp. 103–109, 1995.
7. P. Bonzi, L. E. Depero, F. Parmigiani, C. Perego, and G. Sberveglieri, "Formation and structure of tin iron oxide thin film CO sensors," *J. Material Res.* 9, pp. 1250–1256, 1994.

8. L. E. Depero, F. Parmigiani, C. Perego, G. Sberveglieri, and A. Taroni, "$Sn_{(1-x)}Co_xO_y$: a mixed oxide for carbon monoxide detection," in *Tech. Digest Micro System Technologies '94*, Berlin, Germany, 1994, pp. 439–444.
9. M. Sekimoto, H. Yoshihara, and T. Ohkubo, "Silicon nitride single-layer x-ray mask," *J. Vac. Sci. Technology* 21(4), pp. 1017–1021, 1982.
10. E. I. Bromley, J. N. Randall, D. C. Flanders, and R. W. Mountain, "A technique for the determination of stress in thin films,"*J. Vac. Sci. Technology B* 1, pp. 1364–1366, 1983.
11. M. G. Allen, M. Meheregany, R. T. Howe, and S. D. Senturia, "Microfabricated structures for the in situ measurement of residual stress, Young's modulus, and ultimate strain of thin films," *Appl. Phys. Letter* 51, pp. 241–243, 1987.
12. I. George, P. Carmeli, B. Bonvalot, M. Wagener, A. Girard, A. Zarudiansky, and J. Suski, "Thin membranes with optimized thermomechanical properties for microsystem applications," in *Proc. EUROSENSOR VIII Conf.*, Toulouse, France, 1994, vol. 2, pp. 38–42.
13. S. Moller, J. Lin, and E. Obermeier, "Material and design considerations for low power microheater modules for gas sensor applications," in *Proc. Fifth Int. Meeting on Chemical Sensors*, Rome, Italy, 1994, vol. 1, pp. 433–436.
14. J. G. Korvink, *The SOLIDIS User Manual: Version 1.0*. PEL-ETH Zurich, 1995.
15. E. A. Vittoz, "MOS transistors operated in the lateral bipolar mode and their application in CMOS technology," *IEEE J. Solid-State Circ.* 18, pp. 273–279, 1983.
16. P. E. Allen and D. R. Holberg, *CMOS Analog Circuit Design*. Holt, Rinehart and Winston: New York, NY, USA, 1987.
17. F. Maloberti, "Non conventional signal processing by the use of sigma delta technique: a tutorial introduction," in *Proc. IEEE Int. Symp. on Circ. and Syst.*, San Diego, CA, USA, 1992, pp. 2645–2648.
18. V. F. Dias, "Signal processing in the sigma-delta domain," *Microelectronics Journal* 26, pp. 543–562, 1995.
19. V. Liberali, F. Maloberti, and D. Tonietto, "Sigma-delta processing in multisensor systems for carbon monoxide detection," in *Proc. IEEE Int. Symp. Circ. and Syst.*, Atlanta, GA, USA, 1996, vol. IV, pp. 376–379.
20. F. Op't Eynde, "A power metering ASIC with a sigma-delta-based multiplying ADC," in *IEEE Int. Solid-State Circ. Conf. Dig. of Tech. Papers*, San Francisco, CA, USA, 1994, pp. 186–187.
21. G. van der Horn and J. H. Huijsing, "Smart temperature sensor with integrated bitstream calibration," in *Proc. Eur. Solid-State Circ. Conf.*, Lille, France, 1995, pp. 234–237.
22. N. Kouvaras, "Operations on delta-modulated signals and their application in the realization of digital filters," *Radio and Electronic Engineer* 48, pp. 431–438, 1978.
23. P. O'Leary and F. Maloberti, "A bitstream adder for oversampling coded data," *Electronics Letters* 26, pp. 1708–1709, 1990.
24. P. Malcovati, C. Azeredo Leme, P. O'Leary, F. Maloberti, and H. Baltes, "Smart sensor interface with A/D conversion and programmable calibration," *IEEE J. Solid-State Circ.* 29, pp. 963–966, 1994.
25. The MathWorks, Inc., *MATLAB user's guide*. 1993.
26. V. Liberali, V. F. Dias, M. Ciapponi, and F. Maloberti, "TOSCA: a simulator for switched-capacitor noise-shaping A/D converters," *IEEE Trans. Computer-Aided Design of Integr. Circ. and Syst.* 12, pp. 1376–1386, 1993.

Gian Carlo Cardinali was born in Lugo (Ravenna), Italy, in 1953. He received a degree in electronic engineering from the University of Bologna in 1979. Since October 1979 he has been working at the Lamel Institute of the Italian National research council in Bologna. His scientific interests are in the area of design, fabrication, and testing of semiconductor devices and integrated circuits. He is currently involved in research projects concerning the applicability of microelectronics design methodologies and fabrication technologies to the realization of smart microsensors. He also dealt with physics of photovoltaic conversion and its applications. Now he is head of the Department of Electronics at Lamel Institute.

Leonello Dori joined the CNR-LAMEL Institute in 1969. In 1980, he received the master degree in Physics at the University of Bologna. With the IBM visiting scientist program, he was 4 years at the IBM—Thomas J. Watson Research Laboratory in Yorktown Heights (NY, USA) working on gate dielectric structures of DRAM or Flash memory devices. At the present time he is working on sensor and microsystems R&D program of the LAMEL Institute.

Mauro Fiorini was born in Bologna in 1966. He graduated with Laurea degree in Phisycs from the University of Bologna in 1995. Now he is working at C.N.R. LAMEL institute (Bologna, Italy) with a scholarship from Philips Automation to develop a benzene sensor with Sigma Delta A/D interface.

Isabel Sayago received the Master degree in Physics from the Universidad Complutense de Madrid, in 1993. Since then, she has been working on chemical sensors at the Laboratorio de Sensores (CSIC). She has worked on microsensor at the C.N.R. LAMEL Institute (Bologna, Italy) under a Spanish MEC post-doc program.

Guido Faglia has received an M.S. degree from the Polytechnic of Milan in 1991 with a thesis on gas sensors. Since then he has been studying to obtain the PhD in electronics by the University of Brescia. In 1992 he has been appointed as a Researcher by the Thin Film Lab at the University of Brescia. he is involved in the study of the interactions between gases and the tin oxide surface and in sensor electrical characterization. In 1996 he has received the PhD degree by discussing a thesis on semiconductor gas sensors.

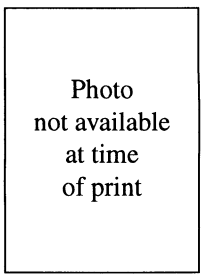

Cesare Perego received his M.S. degree in physics from the University of Milan (Italy) in 1990 discussing a thesis on FTIR and Raman measurements. From 1990 to 1996 he was with the Thin Film Laboratory of the University of Brescia working on the development of solid state sensors. His main interests are in the field of thin layer deposition, and development of gas sensors devices based on mixed oxide. In 1996 he joined Steel Tecnica.

Giorgio Sberveglieri was born in Reggio Emilia, Italy in 1947. In 1968 he received his Diploma degree in Electrical Engineering. In 1970, he joined the Montedison Corporation at the Donegani Research Centre in Novara. In 1987 he was appointed Associate Professor in General Physics at the University of Brescia (Faculty of Engeneering). Since 1987, G. Sberveglieri is leading the Gas Sensor Lab. at the Department of Chemistry and Physics of Material at the same University. In 1994 he became full professor in General Physics and Director of the INFM (National Institute for the Physics of Matter) research unit (18 scientists) at the University of Brescia. G. Sberveglieri's main research interests are on the deposition and electrical characterisation of thin films of gas-sensitive materials using PVD techniques. He has published more than 120 papers in international scientific magazines and congress proceedings on many subjects of material science, particularly on electronic devices based on semiconducting thin films.

Valentino Liberali was born in Broni in 1959. He graduated with the Laurea degree in Electronic Engineering from the University of Pavia in 1986. In the same year he received a one-year scholarship from SGS (now SGS-Thomson Microelectronics), within the frame of the Piano Nazionale Microelettronica. From 1987 to 1990 he was with Italian Nuclear Physics Institute (INFN) working on the development and characterisation of low-noise electronics for particle detectors. In 1990 he joined the Department of Electronics of the University of Pavia, where he worked on the development of the simulator TOSCA for sigma-delta A/D converters. His main research interests are the design of analog/digital interfaces, CAD for analog and mixed integrated circuits and mixed signal testing. V. Liberali is a member of AEI (Associazione Elettrotecnica ed Elettronica Italiana). He has been elected to the Academic Senate of the University of Pavia for the period 1997–1999.

Franco Maloberti received the Laurea Degree in Physics (Summa cum Laude) from the University of Parma in 1968. He joined the University of L'Aquila, then the University of Pavia. For the years 1975–79, he was technical co-ordinator of the Engineering School at the University of Mogadishu, Somalia. He is currently Professor of Microelectronics at the University of Pavia, and is also head of the Micro Integrated Systems Group. His professional expertise is in the design, analysis and characterisation of integrated circuits and analogue digital applications, mainly in the areas of switched capacitor circuits, data converters, interfaces for telecommunication and sensor systems, CAD for analogue and mixed A-D design. Dr. Maloberti has written more than 180 published papers, 2 books and holds 14 patents (2 pending). He was the recipient of the XII Pedriali Prize (1992) for his technical and scientific contributions to national industrial production. He was co-recipient of the IEE Fleming Premium (1996) for the paper "CMOS Triode Transistor Transconductor for high-frequency continuous-time filters". He received the Dr. Honoris Causa in Electronics awarded by Inaoe (Instituto Nacional de Astrofisica, Optica y Electronica), Puebla, Mexico in November 1996. He has been responsible, at both technical and management levels, for many research programmes including 10 ESPRIT projects. He organised the first Special Action for Microelectronics in Italy (I-SMILE, ESPRIT frame); he was the CEC representative in the advisory board of Special Actions I-SMILE, MEPI and SUMIS; he was in the Steering Board of the European Actions EUROCHIP and Combined Action; he was member of the Executive Board of the ESPRIT Project MEDCHIP. Dr. Maloberti also served the European Commission as ESPRIT projects' evaluator and reviewer. He served the Academy of Finland (1996) for the evaluation of the electronic research in Finland. Dr. Maloberti is a member of the AEI (Italian Electrothecnical and Electronic Society), a Fellow of the IEEE (1996), Vice-President Region 8 IEEE-CAS (1995–97), a member of the Editorial Board of Analog Integrated Circuits and Signal Processing, a member of ESSDERC/ESSCIRC Steering Committee, and he was a member of the Steering Committee of the CEC Network NEAR (Network of European Analogue Research).

Davide Tonietto was born in Roma, Italy, in 1970. He received the Laurea Degree in Electronic Engineering from the University of Pavia, Italy, in 1995. In the same year he received a scholarship from INFM, Italy, and he worked on development of an innovative carbon-monoxide smart sensor interface into ESPRIT Project 7500 MEPI.